SCIENTIFIC REPORTS

OPEN

SUBJECT AREAS:
NANOSCIENCE AND TECHNOLOGY
CHEMISTRY

Received
26 September 2013

Accepted
3 June 2014

Published
24 June 2014

Correspondence and requests for materials should be addressed to W.D.X. (wdxiao@iphy.ac.cn) or R.F. (roman.fasel@empa.ch)

Impact of heterocirculene molecular symmetry upon two-dimensional crystallization

W. D. Xiao[1,2], Y. Y. Zhang[2], L. Tao[2], K. Aït-Mansour[1,4], K. Y. Chernichenko[5,6], V. G. Nenajdenko[6], P. Ruffieux[1], S. X. Du[2], H.-J. Gao[2] & R. Fasel[1,3]

[1]Empa, Swiss Federal Laboratories for Materials Science and Technology, 8600 Dübendorf, Switzerland, [2]Institute of Physics, Chinese Academy of Sciences, 100190 Beijing, P.R. China, [3]Department of Chemistry and Biochemistry, Universität Bern, Freiestrasse 3, 3012 Bern, Switzerland, [4]ICMP, Ecole Polytechnique Fédérale de Lausanne, Station 3, 1015 Lausanne, Switzerland, [5]Department of Chemistry, University of Helsinki, P.O. Box 55, 00014, Finland, [6]Department of Chemistry, Moscow State University, Leninskiye Gory, 119992 Moscow, Russia.

Despite the development of crystal engineering, it remains a great challenge to predict the crystal structure even for the simplest molecules, and a clear link between molecular and crystal symmetry is missing in general. Here we demonstrate that the two-dimensional (2D) crystallization of heterocirculenes on a Au(111) surface is greatly affected by the molecular symmetry. By means of ultrahigh vacuum scanning tunneling microscopy, we observe a variety of 2D crystalline structures in the coverage range from submonolayer to monolayer for D_{8h}-symmetric sulflower ($C_{16}S_8$), whereas D_{4h}-symmetric selenosulflower ($C_{16}S_4Se_4$) forms square and rectangular lattices at submonolayer and monolayer coverages, respectively. No long-range ordered structure is observed for C_{1h}-symmetric selenosulflower ($C_{16}S_5Se_3$) self-assembling at submonolayer coverage. Such different self-assembly behaviors for the heterocirculenes with reduced molecular symmetries derive from the tendency toward close packing and the molecular symmetry retention in 2D crystallization due to van der Waals interactions.

It is well known that molecular and crystal symmetries exert great impact on physical properties. However, it has remained a great challenge to predict the three-dimensional (3D) crystal structure even for the simplest molecules, and a clear link between molecular and crystal symmetry is missing in general[1,2]. To reduce complexity, two-dimensional (2D) crystallization through molecular physisorption at surfaces has been intensively studied in recent decades[3–10], as the number of possible motifs for intermolecular interactions and potential packing patterns is greatly reduced due to the planar confinement, allowing deeper understanding of the realization of one possible crystal structure over another[11]. Furthermore, the development of scanning tunnelling microscopy (STM) has enabled the direct imaging of 2D molecular crystals at surfaces with submolecular resolution in real space[12,13], providing direct structural information on crystal lattices along with the molecular arrangement and orientation.

Recently, a statistical analysis on a structural database collecting 2D organic crystals observed by STM at the liquid-solid interface revealed that the tendency toward close packing affects the molecular symmetry retention for various elements[14]. For instance, molecular two-fold rotational symmetry is commonly retained upon 2D crystallization, whereas the molecular mirror plane symmetry is usually lost in 2D crystals[14]. However, most of the molecules that constitute the 2D crystals reported so far are conformationally rather flexible at the liquid-solid interface and include functional groups, which might form directional hydrogen bonds, competing with the molecular close-packing upon 2D crystallization[15–17].

Sulflower, (**1**, $C_{16}S_8$), a planar D_{8h}-symmetric octathio[8]circulene named from sulfur and sunflower, is the first fully heterocyclic circulene[18,19]. Different from the commonly studied thiophene oligomers[20], **1** has an elegant molecular structure of a cycle of eight annulated thiophenic rings and contains no hydrogen atom (Fig. 1). Selenosulflower (**2**, $C_{16}S_4Se_4$), a mixed thiophene-selenophene circulene with reduced D_{4h} symmetry is obtained by replacing the alternate sulfur atoms with four Se atoms in a **1** molecule (Fig. 1)[18,19,21]. As a by-product of **2**, **3** ($C_{16}S_5Se_3$) with three selenium atoms and five sulfur atoms shows a C_{1h} symmetry (Fig. 1)[18,19,21]. As all atoms of molecules **1**, **2** and **3** are chemically saturated, without any hydrogen atom and functional group, intermolecular interactions are dominated by van der Waals (vdW) forces. These three molecules thus constitute an excellent

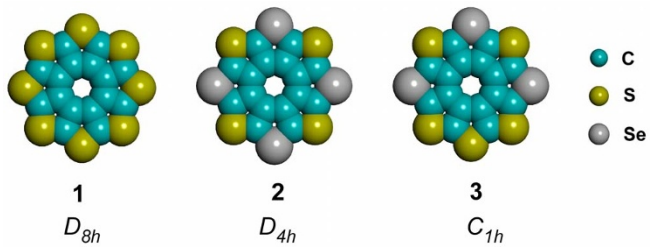

Figure 1 | Molecular structures of heterocirculenes 1–3 showing identical planar disk-shaped geometries but reduced symmetries.

family of rigid heterocirculenes with planar disk-shaped geometry but different symmetries, which provides an ideal model system to investigate the interplay between molecular and crystal symmetries upon 2D crystallization.

The 3D crystal structures of **1** and **2** have been characterized by X-ray diffraction[18,22–24]. Despite their high molecular symmetries, both **1** and **2** crystallize in a similar non-centrosymmetric $P2_1$ space group[18,22–24], except that a rotational disorder is observed for **2**[24]. Recently, **1** and **2** were imaged by STM at submolecular level after their accommodation and immobilization by trimesic acid (TMA) honeycomb networks at the solution-graphite interface[24]. However, the intrinsic interfacial structure of **1** and **2** on solid surfaces remains unclear, due to the presence of foreign molecules[24].

In this work, we report on the 2D crystallization of heterocirculenes **1**–**3** on Au(111) as investigated by means of ultrahigh vacuum (UHV) STM. We observe a variety of 2D crystalline structures in the coverage range from submonolayer to monolayer for **1**, whereas **2** forms square and rectangular lattices at submonolayer and monolayer coverages, respectively. No long-range ordered structure is observed for **3** self-assembling at submonolayer coverage. Such different self-assembly behaviors for the heterocirculenes with reduced molecular symmetries show the tendency toward close packing and the molecular symmetry retention in 2D crystallization due to vdW interactions.

Results

The clean Au(111) surface exhibits a well-known $22 \times \sqrt{3}$ herringbone reconstruction, consisting of a series of parallel zigzag ridges long the <11-2>-directions on terraces, which are discommensuration lines separating wider face-centered cubic (fcc) and narrower hexagonal close-packed (hcp) stacking regions[25]. After vapor deposition of ~0.1 monolayer (ML) of **1** on an atomically clean Au(111) surface at room temperature, we observe by STM (~40 K) a variety of ordered molecular islands with straight edges as well as disordered molecular aggregates with zigzag edges (Fig. 2a). Each molecule on the flat terraces of Au(111) exhibits a ring protrusion and a depression at the center (Fig. 2b), suggesting that the planar skeleton of the molecule is parallel to the metal surface due to the molecule-substrate interaction. An STM simulation based on density functional theory (DFT) calculations (Inset of Fig. 2a) reproduces the STM images very well, and reveals that the ring protrusion originates from the sulfur atoms of the molecular skeleton. This feature is in contrast to the 'circle with eight petals' appearance of **1** when it is trapped in the pores of a TMA network at the solution-graphite interface[24]. As each sulfur atom of **1** is chemically saturated in a five-member ring with significant aromaticity[26,27], the molecule-substrate interaction mainly derives from the coupling between the molecular π-electrons and the metal, akin to the planar polycyclic aromatic hydrocarbon molecules on Au(111) and in contrast to the strong S-Au bonding widely reported for thiols adsorbed on gold substrates[3–10,28–31]. This molecule-substrate interaction is rather weak, as evidenced by frequent displacements of the molecules due to the disturbance exerted by STM tips during scanning with normal tunnelling parameters.

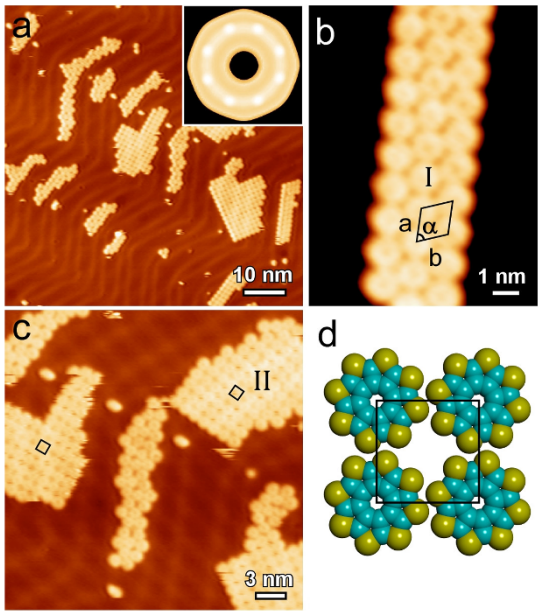

Figure 2 | Small molecular aggregates, narrow belt-shaped islands and extended islands of 1 on Au(111) at ~0.1 ML coverage. (a) Large-scale STM image. The inset shows a simulated STM image of **1** based on DFT calculations. (b) Zoom-in showing the oblique lattice (phase I) of a narrow belt-shaped island. (c) Zoom-in showing several extended molecular islands with a square lattice (phase II) and disordered molecular aggregates. (d) Structural model of the square lattice seen in (c).

This weak interaction is also confirmed by state-of-the-art *ab initio* vdW-DF calculations (see Supplementary Information).

The ordered molecular islands showing a narrow belt shape with straight edges nearly parallel to the discommensuration lines along the <11-2>-directions (with a small angle of $6^\circ \pm 2^\circ$) are exclusively located in the fcc domains of the Au(111) surface. This preferential adsorption behavior indicates a higher surface interaction in the fcc regions than in the hcp ones. This can be understood on the basis of a different electronic potential energy, reported to be 25 meV higher for the fcc regions than for the hcp regions of the Au(111)-$22 \times \sqrt{3}$ superstructure[32], which influences the respective adsorption energies[33]. Zoom-in STM images (Fig. 2b) show that these islands illustrate an oblique superlattice (phase I) with a unit cell described by $a = 1.09 \pm 0.05$ nm, $b = 1.16 \pm 0.05$ nm and $\alpha = 65^\circ \pm 5^\circ$. Extended molecular islands that cross the discommensuration lines and occupy several fcc and hcp domains usually illustrate a square periodicity (phase II) with $a = 1.04 \pm 0.05$ nm, as seen in Fig. 2c. Direct determination of the molecular orientations is not achieved, since the molecules appear as featureless rings in the STM images, leading to an uncertainty of a plane group of either *p4* or *p4mm* for the square lattice. Figure 2d shows the proposed structural model of the square lattice of **1**.

At a coverage of ~0.4 ML, the molecular islands of **1** cross the discommensuration lines of Au(111) and grow into large domains exhibiting an oblique superlattice (phase III) with $a = 1.03 \pm 0.05$ nm, $b = 1.06 \pm 0.05$ nm and $\alpha = 68^\circ \pm 5^\circ$, as shown in Fig. 3a. The structural model of this oblique lattice is depicted in Fig. 3c. Small patches with square periodicity can also be observed at this coverage. Increasing the coverage to ~0.8 ML leads to the growth of phase III islands and the complete suppression of the square structure.

Figure 3b shows the molecular adlayer observed after deposition of 1 ML of **1**. The molecules form a hexagonal close-packed layer with nearest neighbor distances of 1.07 ± 0.05 nm (phase IV). Careful analysis unveils that the lattice vectors **a** and **b** are parallel to the

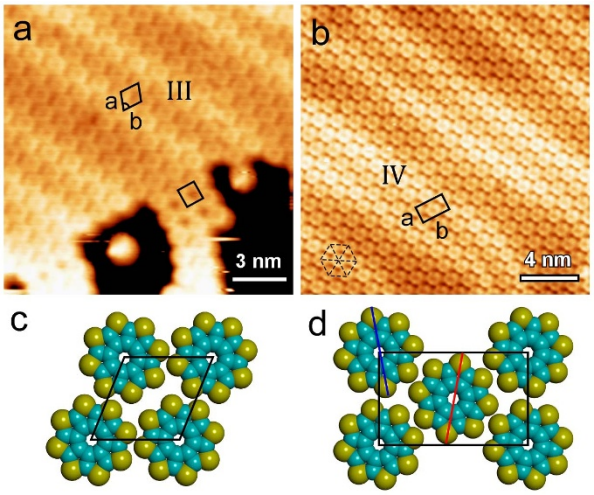

Figure 3 | Intermediate and high coverage phases of 1 on Au(111). (a) STM image showing the co-existence of extended molecular islands with an oblique lattice (phase III) and a small patch with a square lattice at ~0.4 ML coverage of **1**. (b) STM image of complete molecular layer of **1** on Au(111) showing a centered rectangular lattice (phase IV). (c,d) Structural models of the oblique and rectangular lattices seen in (a,b), respectively.

<110> and <11-2>-directions of the Au(111) surface, respectively. The observed intermolecular spacing and lattice orientation are compatible with a commensurate (4 × 4) superstructure. If we consider the possibility of non-equivalent azimuthal orientations for alternating molecules within the close-packed layer, as detailed below, the corresponding superlattice is a centered rectangular one with lattice constants a = 1.07 ± 0.05 nm and b = 1.86 ± 0.05 nm, as indicated in Fig. 3b,d. It can be expressed by the superstructure matrix

$$\begin{pmatrix} a \\ b \end{pmatrix} = \begin{pmatrix} 4 & 0 \\ -4 & 8 \end{pmatrix} \bullet \begin{pmatrix} a_0 \\ b_0 \end{pmatrix}$$

where $\mathbf{a_0}$ and $\mathbf{b_0}$ are the primitive lattice vectors of the Au(111) surface. If the two molecules of the unit cell adopt different azimuthal orientations, as evidenced by our calculations (see below), the superlattice of the full monolayer of **1** is described by the plane group *p2gg*, similar to the monolayer structure of **2** discussed below. Figure 3d illustrates the corresponding structural model of the rectangular lattice of the full monolayer of **1**.

In contrast to **1**, STM measurements at ~40 K disclose no additional structure except the characteristic features of the Au(111)-22 × $\sqrt{3}$ superstructure at a submonolayer coverage of **2**. This indicates a higher mobility and weaker molecule-substrate interaction for **2** adsorbed on Au(111). However, extended molecular islands illustrating a square lattice, as well as disordered molecular aggregates, are observed for D_{4h}-symmetric **2** at ~5 K. This clearly differs from the series of phase transitions of D_{8h}-symmetric **1** upon crystallization with increasing molecular coverage. Figure 4a shows a typical STM image taken after deposition of ~0.4 ML of **2** onto Au(111). Extended molecular islands are observed to cross the discommensuration lines of the Au(111) surfaces. High-resolution STM images of the extended molecular islands unveil a square lattice with a lattice parameter of a = 1.07 ± 0.05 nm, as shown in Fig. 4b,c. Different than the ring-shaped STM topographs of the D_{8h}-symmetrical molecules **1**, **2** is imaged as a square with four protrusions located at the corners (Fig. 4b,c), consistent with the molecular D_{4h} symmetry and a flat adsorption configuration due to the weak molecule-substrate interaction. The STM image of **2** is well reproduced by simulations based on DFT calculations (Inset of Fig. 4a), which disclose that the four protrusions originate from the selenium atoms of the molecular skeleton. This square shaped feature with four protrusions for each

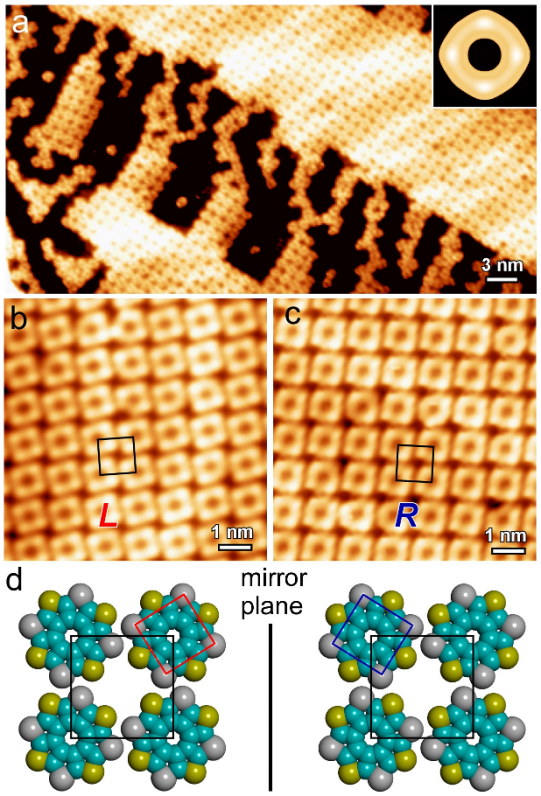

Figure 4 | Extended islands and disordered molecular aggregates of 2 on Au(111) at ~0.4 ML coverage. (a) Large-scale STM image. The inset shows a simulated STM image of **2** based on DFT calculations. (b,c) High resolution STM images revealing the handedness of the square lattice of **2**. (d) Structural models of the chiral square lattices seen in (b,c), respectively.

molecule of **2** is different from the 'circle with eight petals' that **2** shows when it is trapped in the pores of a TMA network at the solution-graphite interface[24]. We note that the high-symmetry axes of **2** are rotated away from the lattice vectors of the molecular superlattice by ~12° ± 2°, resulting in a *p4* plane group. Although **2** is achiral, this induces 2D chirality into the molecular islands. Figure 4d shows structural models of the chiral square lattices of **2**.

At a coverage of 1 ML, a quasi-hexagonal close-packed layer of **2** is formed. Due to clearly alternating azimuthal molecular orientations within the layer, it must be described by a centered rectangular lattice with a unit cell containing two molecules, with lattice parameters a = 1.12 ± 0.05 nm and b = 1.82 ± 0.05 nm, as indicated in Fig. 5a. This rectangular superlattice is compatible with the (4 0–4 8) unit cell derived for the close-packed monolayer of **1** and the *p2gg* plane group. A corresponding structural model of the lattice is shown in Fig. 5b.

For molecule **3** adsorbed on Au(111) at submolecular coverage, e.g. at ~0.3 ML, no long-range ordered structures are observed by STM down to sample temperature of ~5 K, as seen in Fig. 6a. Each molecule **3** appears as a pentagon with three protrusions brighter than the other two, consistent with its C_{1h} symmetry. The simulated STM image based on DFT calculations is in line with this topographic feature (Inset of Fig. 6a), and unveils that the three brighter protrusions are due to the three selenium atoms, while the other two are attributed to two sulfur atoms. Despite the lack of long-range order in the molecular aggregates of **3**, locally well-defined supramolecular structures, such as chiral trimers, can be distinguished, as shown in Fig. 6b. The chiral trimers constitute building blocks and finally build up the main feature of the disordered aggregates of **3**. Figure 6c shows the structural models of the chiral trimers of **3**.

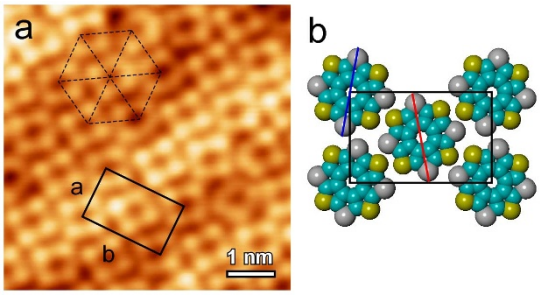

Figure 5 | Close-packed monolayer of 2 on Au(111). (a) STM image showing a centered rectangular lattice of the close-packed monolayer. (b) Structural models of the rectangular lattice.

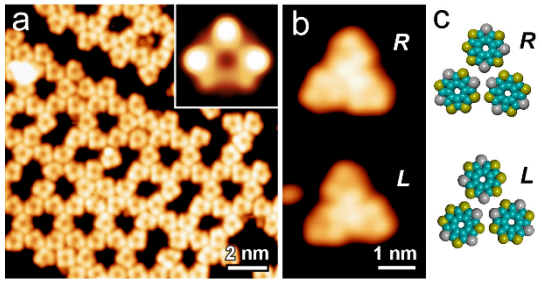

Figure 6 | Disordered molecular aggregates of 3 on Au(111) at a coverage of ~0.3 ML. (a) STM image. The inset shows the simulated STM image of **3** based on DFT calculations. (b) STM image of two trimers of **3** exhibiting different chirality. (c) Structural models of the chiral trimers shown in (b).

Discussion

We have calculated the molecular density of the various ordered phases of **1** using the measured lattice parameters, and find that it increases in the sequence of phase I < phase II < phase III < phase IV. This suggests that the series of phase transitions of **1** on Au(111) is mainly driven by the propensity to molecular close-packing. A similar mechanism also accounts for the phase transition from a square lattice to a centered rectangular one for 2D crystallization of **2**. Therefore, the observed coverage-dependant phase transitions of **1** and **2** can be rationalized by Kitaigorodskii's principle of close-packing[34]. This is reasonable as the intermolecular interaction is dominated by vdW forces (see below) for both heterocirculenes **1** and **2**, which favors molecular close-packing during crystallization. It is noteworthy that the centered rectangular lattices of **1** and **2** on Au(111) at monolayer coverage are very similar to the (100) surfaces of **1** and **2** in the bulk crystal[18,22,24], except that both **1** and **2** are tilted in the bulk, while they adopt flat configurations on Au(111) due to the weak but non-negligible molecule-substrate interaction. Indeed, centered rectangular lattices with tilted molecular configurations are observed in the second layer of **1** (Supplementary Fig. 2) on Au(111) surface, as the interaction between the molecules of the second layer and the substrate has been distinctly weakened by the screening effect of the first layer.

To shed further light on the self-assembly of **1**, **2** and **3** on Au(111), we have performed state-of-the-art *ab initio* vdW-DF calculations. Compared to the commonly used functionals based on generalized gradient approximations (GGA), the vdW-DF method improves the description of vdW interactions. As on one hand our experiments and calculations (Supplementary Information) reveal weak molecule-substrate interactions, and on the other hand the self-assembly patterns (except the centered rectangular lattices) are incommensurate to the substrate that exhibits the herringbone reconstruction, we only consider free-standing molecular layers in our calculations. These reveal that the energetically most favorable 2D crystal structure of **2** is a rectangular lattice with two non-equivalent molecules in each unit cell (Fig. 5b). For one configuration of **2**, the C_{4v} axes across two Se atoms are rotated away from the lattice vectors of the molecule superlattice by $+11^\circ$, while for the other configuration, this azimuthal angle is -11° (Fig. 5b). An interaction energy of -0.37 eV per molecule is obtained. The calculated lattice parameters are a = 1.17 nm and b = 1.84 nm, which are consistent with the experimental values. A meta-stable configuration is found with a square lattice. In this configuration, molecules are separated by 1.11 nm, which is also in good agreement with the experimental observations. The corresponding interaction energy per molecule is -0.17 eV, and thus higher than that of the rectangular lattice. In particular, our calculations unveil that the C_{4v} axes across two Se atoms of **2** are rotated away from the lattice vectors of the molecule superlattice by $\sim 13^\circ$ (Fig. 4d), consistent with the experimental observation of $\sim 12^\circ$. Similarly, a rectangular lattice with two non-equivalent molecules in each unit cell (Fig. 3d) is found to be the most stable 2D structure of **1** according to our calculations (interaction energy of -0.36 eV per molecule). The calculated lattice parameters are a = 1.12 nm and b = 1.83 nm, consistent with those of the experimental observations. An oblique lattice of **1** is obtained if we constrain each unit cell to include only one molecule. The lattice parameters of the optimized oblique lattice are a = 1.06 nm, b = 1.07 nm and $\alpha = 68^\circ$, in line with the oblique lattice of phase III. The calculated interaction energy is -0.28 eV per molecule, and thus higher than that of the centered rectangular lattice. Finally, a square lattice with an intermolecular separation of 1.07 nm (Fig. 2d) is disclosed for **1** with the constraint of a rectangular unit cell containing a single molecule (interaction energy of -0.20 eV per molecule). The formation of chiral trimers of **3** is also reproduced, as seen in Fig. 6c. The calculated intermolecular distance and interaction energy per trimer are 1.18 nm and -0.37 eV per trimer, respectively. We propose that the formation of trimers and porous structures is due to the 3-fold symmetric substrate. Notably, we compared the interaction energies obtained with the vdW-DF and the GGA functionals (Perdew-Burke–Ernzerhof, i.e. PBE). Our results show that vdW interactions contribute to more than 90% of the interaction energy. In plots of the electron localization function (ELF) and electron density difference, which are often used to determine formation of bonds, we find no evidence for strong S···S interaction between adjacent molecules (Supplementary Information). The interaction between heterocirculenes is thus dominated by vdW interactions, different than the strong S···S interaction that e.g. directs the formation of porous networks of the fused thiophene derivative *trans*-1,2-(dithieno[2,3-*b*:3′,2′-*d*]-thiophene)ethene (TDT) at the solid-liquid interface[35].

Despite the successful reproduction of the experimentally observed lattice structures, the interaction energy calculations alone cannot explain the coverage-dependent structural evolution of **1** and **2**, suggesting that molecule-substrate interactions, which are not considered in our calculations due to the incommensurability between the self-assembled molecular patterns and the Au(111) substrate, play an important role in the 2D crystallization of the heterocirculene molecules. Indeed, direct evidence for impact of the substrate is given by the observed tendency towards structures that are aligned along particular high-symmetry directions of the Au(111) substrate surface or even commensurate to Au(111). However, accurate calculations taking both molecule-molecule and molecule-substrate interactions into account are beyond the computational capability, due to the generally incommensurate lattices of the molecular layer and the Au(111) substrate.

Nevertheless, the distinctly different self-assembly behaviors of **1**, **2** and **3** on Au(111) demonstrate that the molecular symmetry exerts great impact upon the 2D crystallization of the heterocirculene molecules. As the vdW interaction between the heterocirculene molecules is the main driving force for 2D crystallization and close-packing, the different self-assembly behaviors indicate that the intermolecular

vdW interaction is strongly related to the molecular geometry. In fact, the molecular vdW surface directly reflects the molecular symmetry. During 2D crystallization, neighboring molecules tend to arrange their positions and orientations in order to get their molecular vdW surfaces contacted as much as possible, resulting in a tendency to retain the highest rotational symmetry of the molecules in the 2D crystal. Meanwhile, the preferential orientation of the molecules with respect to the substrate is determined by the molecule-substrate interaction, entailing symmetry mismatch between the molecular adsorbates (D_{8h} and D_{4h} for **1** and **2**, respectively) and the Au(111) substrate (C_{3v}). A subtle interplay of molecule-molecule and molecule-substrate interactions then leads to the formation of different lattice structures for increasing coverages of **1** and **2**. As the molecular symmetry of **1** is higher than that of **2** and the vdW surface of **1** is close to an isotropic circle, more metastable structures with (almost) degenerate energies might be formed during 2D crystallization of **1**, resulting e.g. in the appearance of an oblique lattice for **1** whereas a similar structure is not observed for **2**.

In summary, we have investigated the 2D crystallization of three closely related heterocirculenes on Au(111) by means of UHV STM. We observe a variety of 2D crystalline structures in the coverage range from submonolayer to monolayer for **1**, whereas **2** forms square and rectangular lattices at submonolayer and monolayer coverages, respectively. No long-range ordered structure is observed for **3** self-assembling at submonolayer coverage. The distinctly different self-assembly behaviors of the heterocirculenes with reduced molecular symmetries evidence a clear tendency toward close-packing and molecular symmetry retention upon 2D crystallization due to vdW interactions. This work clearly shows how the symmetry of a molecular monomer can impact the symmetry of the resulting 2D crystal, but also highlights the importance of concurrent molecule-substrate interactions.

Methods

Experimental method. Experiments were performed in two independent UHV systems (base pressure $\sim 1 \times 10^{-10}$ mbar). One system housed a commercial variable temperature STM (VT-STM) and the other a low-temperature STM (LT-STM) (Omicron Nanotechnology GmbH), both equipped with standard surface preparation facilities. The Au(111) surface was prepared by repeated cycles of sputtering with argon ions and annealing at 450°C. Before deposition of heterocirculenes, cleanliness and surface order were monitored by STM and low-energy electron diffraction. The heterocirculenes were deposited via vacuum sublimation from a Knudsen-type evaporator with the sample held at room temperature. Prior to deposition, **1** and **2** were purified via vacuum sublimation, as described elsewhere[18,19,21]. The by-products of **2**, such as **3** and its isomers, cannot be efficiently separated from **2**[19]. We find, however, that **2** and **3** can be selectively deposited, since they sublimate at somewhat different temperatures, due to different molecular masses[19]. One monolayer (ML) refers to a molecular density of 1 molecule/nm^2, corresponding to the completion of an ordered heterocirculene layer with a centered rectangular lattice on Au(111), as judged with STM. All STM images were acquired in constant-current mode either at a sample temperature of ~40 K for **1** (VT-STM) or at ~5 K (LT-STM) for **2** and **3**.

Calculation details. Quantum mechanical calculations based on density functional theory (DFT) were performed using the Vienna *ab initio* simulation package (VASP)[36,37]. The projector augmented wave method and vdW-DF proposed by Langreth and Lundqvist were employed[38–43]. Energy cutoff for the plane waves was 400 eV. Molecular structures were fully relaxed with the net force smaller than 0.01 eV/Å on all atoms. Lattice constants of the self-assembly patterns are relaxed until a stress smaller than 0.25 kilobar. k-point sampling in the Brillouin zone is carefully tested and binding energies are converged to 0.01 eV. STM images were simulated within the Tersoff-Hamann approach[44].

1. Dunitz, J. D. Are crystal structures predictable? *Chem. Comm.* 545–548 (2003).
2. Desiraju, G. R. Cryptic crystallography. *Nature Mater.* **1**, 77–79 (2002).
3. Barth, J. V. Molecular Architectonic on Metal Surfaces. *Annu. Rev. Phys. Chem.* **58**, 375–407 (2007).
4. Elemans, J. A. A. W., Lei, S. & De Feyter, S. Molecular and Supramolecular Networks on Surfaces: From Two-Dimensional Crystal Engineering to Reactivity. *Angew. Chem. Int. Ed.* **48**, 7298–7332 (2009).
5. Bartel, L. Tailoring molecular layers at metal surfaces. *Nature Chem.* **2**, 87–95 (2010).
6. Bonifazi, D., Mohnani, S. & Llanes-Pallask, A. Supramolecular Chemistry at Interfaces: Molecular Recognition on Nanopatterned Porous Surfaces. *Chem. Eur. J* **15**, 7004–7025 (2009).
7. Liang, H. *et al.* Two-dimensional molecular porous networks constructed by surface assembling. *Coord. Chem. Rev.* **253**, 2959–2979 (2009).
8. Ciesielski, A., Palma, C.-A., Bonini, M. & Samori, P. Towards supramolecular engineering of functional nanomaterials: pre-programming multi-component 2D self-assembly at solid-liquid interfaces. *Adv. Mater.* **22**, 3506–3520 (2010).
9. Slater, A. G., Beton, P. H. & Champness, N. R. Two-dimensional supramolecular chemistry on surfaces. *Chem. Sci.* **2**, 1440–1448 (2011).
10. Otsuki, J. STM studies on porphyrins. *Coord. Chem. Rev.* **254**, 2311–2341 (2010).
11. Plass, K. E., Kim, K. & Matzger, A. J. Two-dimensional crystallization: self-assembly, pseudopolymorphism, and symmetry-independent molecules. *J. Am. Chem. Soc.* **126**, 9042–9053 (2004).
12. De Feyter, S. & De Schryver, F. C. Two-dimensional supramolecular self-assembly probed by scanning tunneling microscopy. *Chem. Soc. Rev.* **32**, 139–150 (2003).
13. Rosei, F. *et al.* Properties of large organic molecules on metal surfaces. *Prog. Surf. Sci.* **71**, 95–146 (2003).
14. Plass, K. E., Grzesiak, A. L. & Matzger, A. J. Molecular packing and symmetry of two-dimensional crystals. *Acc. Chem. Res.* **40**, 287–293 (2007).
15. Schmidt, G. M. J. Photodimerization in the solid state. *Pure Appl. Chem.* **27**, 647–678 (1971).
16. Desiraju, G. R. Supramolecular Synthons in Crystal Engineering—A New Organic Synthesis. *Angew. Chem. Int. Ed.* **34**, 2311–2327 (1995).
17. Su, D., Wang, X., Simard, M. & Wuest, J. D. Molecular tectonics. *Supramol. Chem.* **6**, 171–178 (1995).
18. Chernichenko, K. Y. *et al.* "Sulflower": A New Form of Carbon Sulfide *Angew. Chem. Int. Ed.* **45**, 7367–7370 (2006).
19. Chernichenko, K. Y., Balenkova, E. S. & Nenajdenko, V. G. From thiophene to Sulflower. *Mend. Comm.* **18**, 171–179 (2008).
20. Torroba, T. & García-Valverde, M. Rigid Annulated Carbon–Sulfur Structures. *Angew. Chem. Int. Ed.* **45**, 8092–8096 (2006).
21. Dadvand, A. *et al.* Heterocirculenes as a new class of organic semiconductors. *Chem. Commun.* 5354–5356 (2008).
22. Fujimoto, T., Suizu, R., Yoshikawa, H. & Awaga, K. Molecular, Crystal, and Thin-Film Structures of Octathio[8]circulene: Release of Antiaromatic Molecular Distortion and Lamellar Structure of Self-Assembling Thin Films. *Chem. Eur. J.* **14**, 6053–6056 (2008).
23. Bukalov, S. S. *et al.* Two Modifications Formed by "Sulflower" $C_{16}S_8$ Molecules, Their Study by XRD and Optical Spectroscopy (Raman, IR, UV−Vis) Methods. *J. Phys. Chem. A* **112**, 10949–10961 (2008).
24. Ivasenko, O. *et al.* Supramolecular assembly of heterocirculenes in 2D and 3D. *Chem. Commun.* 1192–1194 (2009).
25. Barth, J. V., Brune, H., Ertl, G. & Behm, R. J. Scanning tunneling microscopy observations on the reconstructed Au(111) surface: Atomic structure, long-range superstructure, rotational domains, and surface defects. *Phys. Rev. B* **42**, 9307–9318 (1990).
26. Datta, A. & Pati, S. K. Computational Design of High Hydrogen Adsorption Efficiency in Molecular "Sulflower" *J. Phys. Chem. C* **111**, 4487–4490 (2007).
27. Gahungu, G. & Zhang, J. Shedding light on octathio[8]circulene and some of its plate-like derivatives. *Phys. Chem. Chem. Phys.* **10**, 1743–1747 (2008).
28. Ruffieux, P. *et al.* Self-Assembly of Extended Polycyclic Aromatic Hydrocarbons on Cu(111). *J. Phys. Chem. B* **110**, 11253–11258 (2006).
29. Nion, A., Jiang, P., Popoff, A. & Fichou, D. Rectangular Nanostructuring of Au(111) Surfaces by Self-Assembly of Size-Selected Thiacrown Ether Macrocycles. *J. Am. Chem. Soc.* **129**, 2450–2451 (2007).
30. Bashir, A. *et al.* Selenium as a Key Element for Highly Ordered Aromatic Self-Assembled Monolayers. *Angew. Chem. Int. Ed.* **47**, 5250 (2008).
31. Hohman, J. N. *et al.* Dynamic Double Lattice of 1-Adamantaneselenolate Self-Assembled Monolayers on Au{111}. *J. Am. Chem. Soc.* **133**, 19422–19431 (2011).
32. Chen, W., Madhavan, V., Jamneala, T. & Crommie, M. F. Scanning Tunneling Microscopy Observation of an Electronic Superlattice at the Surface of Clean Gold. *Phys. Rev. Lett.* **80**, 1469–1472 (1998).
33. Xiao, W. D. *et al.* Formation of a Regular Fullerene Nanochain Lattice. *J. Phys. Chem. B* **110**, 21394–21398 (2006).
34. Kitaigorodskii, A. I. The principle of close packing and the condition of thermodynamic stability of organic crystals. *Acta Crystallogr.* **18**, 585–590 (1965).
35. Wang, X.-Y. *et al.* Molecular evidence for the intermolecular S···S interaction in the surface molecular packing motifs of a fused thiophene derivative. *Chem. Commun.* **49**, 1829–1831 (2013).
36. Kresse, G. & Hafner, J. *Ab initio* molecular dynamics for liquid metals. *Phys. Rev. B* **47**, 558–561 (1993).
37. Kresse, G. & Furthmüller, J. Efficient iterative schemes for *ab initio* total-energy calculations using a plane-wave basis set. *Phys. Rev. B* **54**, 11169–11186 (1996).
38. Perdew, J. P., Burke, K. & Ernzerhof, M. Generalized Gradient Approximation Made Simple. *Phys. Rev. Lett.* **77**, 3865–3868 (1996).
39. Blöchl, P. E. Projector augmented-wave method. *Phys. Rev. B* **50**, 17953–17979 (1994).
40. Kresse, G. & Joubert, D. From ultrasoft pseudopotentials to the projector augmented-wave method. *Phys. Rev. B* **59**, 1758–1775 (1999).

41. Medeiros, P. V. C., Gueorguiev, G. K. & Stafström, S. Benzene, coronene, and circumcoronene adsorbed on gold, and a gold cluster adsorbed on graphene: Structural and electronic properties. *Phys. Rev. B* **85**, 205423 (2012).
42. Langreth, D. C. *et al.* Van der Waals density functional theory with applications. *Int. J. Quantum Chem.* **101**, 599–610 (2005).
43. Dion, M., Rydberg, H., Schröder, E., Langreth, D. C. & Lundqvist, B. I. Van der Waals Density Functional for General Geometries. *Phys. Rev. Lett.* **92**, 246401 (2004).
44. Tersoff, J. & Hamann, D. R. Theory of the scanning tunneling microscope. *Phys. Rev. B* **31**, 805–813 (1985).

Acknowledgments

Financial support by the European Commission, the Swiss National Science Foundation and the National Natural Science Foundation of China is gratefully acknowledged. Supercomputer time was provided by the XSEDE Science Gateways program.

Author contributions

W.D.X., K.A.-M. and P.R. performed STM measurements. Y.Y.Z., L.T., S.X.D. and H.-J.G. conducted DFT calculations. K.Y.C. and V.G.N. synthesized and purified the molecules. W.D.X., Y.Y.Z. and R.F. analyzed the data and wrote the manuscript. R.F. designed and coordinated the project. All authors discussed the results and commented on the manuscript.

Additional information

Supplementary information accompanies this paper at http://www.nature.com/scientificreports

Competing financial interests: The authors declare no competing financial interests.

How to cite this article: Xiao, W.D. *et al.* Impact of heterocirculene molecular symmetry upon two-dimensional crystallization. *Sci. Rep.* **4**, 5415; DOI:10.1038/srep05415 (2014).